POLITECNICO DI TORINO
Repository ISTITUZIONALE

On the influence of the elastic characteristics of composite materials on the vibrating properties

Original
On the influence of the elastic characteristics of composite materials on the vibrating properties / Risitano, Giacomo; Scappaticci, Lorenzo; Alberti, Fabio; Santonocito, Dario; D'Andrea, Danilo. - In: JOURNAL OF VIBRATION AND CONTROL. - ISSN 1077-5463. - ELETTRONICO. - 29:15-16(2022), pp. 3387-3400. [10.1177/10775463221098228]

Availability:
This version is available at: 11583/2985338 since: 2024-02-07T14:33:49Z

Publisher:
SAGE Publications Ltd STM

Published
DOI:10.1177/10775463221098228

Terms of use:

This article is made available under terms and conditions as specified in the corresponding bibliographic description in the repository

Publisher copyright
Common Ground Research Network postprint versione editoriale/Version of Record, con licenza CC by nc

Risitano, Giacomo; Scappaticci, Lorenzo; Alberti, Fabio; Santonocito, Dario; D'Andrea, Danilo(2022). On the influence of the elastic characteristics of composite materials on the vibrating properties in : JOURNAL OF VIBRATION AND CONTROL, 29, 15-16, 3387-3400, http://doi.org/10.1177/10775463221098228 © Common Ground Research Networks, Authors, Some Rights Reserved, (CC BY-NC-ND 4.0). Permissions:

(Article begins on next page)

12 May 2024

Check for updates

Review

Journal of Vibration and Control
2022, Vol. 0(0) 1–14
© The Author(s) 2022
Article reuse guidelines:
sagepub.com/journals-permissions
DOI: 10.1177/10775463221098228
journals.sagepub.com/home/jvc
SAGE

On the influence of the elastic characteristics of composite materials on the vibrating properties

Giacomo Risitano[1], Lorenzo Scappaticci[2], Fabio Alberti[1], Dario Santonocito[1] and Danilo D'Andrea[1]

Abstract

Economical composite materials such as PA66GF35 (glass-fibre-reinforced polyamide matrix) are being increasingly used in the automotive industry. Their good mechanical characteristics combined with low density, very high workability, low production cost and high availability are attractive prerogatives that induce engineers to adopt it in complex technological challenges. Injection moulding is the most common production technology used to realize composite components. While in industrial design this type of material is considered as isotropic, it is well known that injection moulding process gives orientation to the reinforcing fibres, leading to anisotropic mechanical behaviour. Starting from these considerations, attention has been turned to the vibrating properties of such materials and to the comparison between vibration modes and mechanical properties. In fact, composite materials are also used to produce components in the automotive field significantly affected by noise problems. Since the noise derives from a fluid-structure interaction, the own frequencies and the vibrating modes cover an important role on the Noise, Vibration and Harshness performance of the components. A comparison of the vibration modes of a plate in PA66GF35, numerically modeled both as isotropic and anisotropic material according to Folgar and Tucker theory, was carried out and compared with experimental measurements. The anisotropy of the composite material is demonstrated by the variation of the mechanical characteristics obtained from the static tensile tests. Results show that injection moulding confers different mechanical properties to real components due to the intrinsic fluid-dynamic phenomena of the production process.

Keywords

Composite materials, modal analysis, cantilever plate vibration, noise, vibration and harshness

1. Introduction

Short-fibre reinforced thermoplastic composites have good structural characteristics, also in consideration of their density (Treviso et al., 2015; Vaidya and Chawla, 2008; Wu et al., 2001). Further qualities, such as excellent workability, availability and recyclability together with their low cost, are attractive features that justify their widespread diffusion in the automotive and naval field (Anandakumar et al., 2021; Cucinotta et al., 2016; Inoue et al., 2019; Launay et al., 2010; Mouti et al., 2010).

Most components in reinforced thermoplastic material are realized by injection moulding (Bigg, 1985; Caltagirone et al., 2021; Fu et al., 2020; Ye et al., 2008). It is an industrial production process in which a plastic material is melted, mixed with reinforcing short glass fibres and subsequently injected into a closed mould at high pressure. Such a technological process makes the modeling of the mechanical behaviour of the material tricky. The reinforcing fibres dispersed in the matrix, in fact, are not arranged neatly, as in the case of long-fibre composites, but are distributed stochastically (Lopes et al., 2010; Martinez and Bishay, 2021; Onkar et al., 2007; Tawfik et al., 2018) as a function of the thermo-fluid-dynamic phenomena that occur inside the mould. This essentially means that the mechanical characteristics of the finished product depend on the casting conditions (temperature of the cast, flow velocity and outlet section) and also on the geometric

[1]Department of Engineering, University of Messina, Messina, Italy
[2]Allimep srl, Perugia, Italy

Received: 13 November 2021; accepted: 15 April 2022

Corresponding author:
Danilo D'Andrea, Department of Engineering, University of Messina, Contrada di Dio (S. Agata), Messina 98166, Italy.
Email: danilo.dandrea@unime.it

position of the injection point, or points, of the mould (Kuo et al., 2009; Mortazavian and Fatemi, 2015). Indeed, due to the constituents' nature and production process, the reinforced polymers are in most cases characterized by a certain anisotropy (Bernasconi et al., 2008; Hao et al., 2020; Hmeidat et al., 2020), generally difficult to deal with during component design, since the shape of the dispersed fibres and the production process confer a directionality that defines peculiar prerogatives to the mechanics of the material (Bernasconi et al., 2007; De Monte et al., 2010). In terms of structural dynamics, neglecting such a 'directional behaviour' of the material may also mean underestimating vibrational phenomena of the components themselves (Gibson, 2000). Always more frequently, in fact, such materials are used to manufacture automotive components, as for the case of engine subsystems (Mouti et al., 2010) (e.g. air intake manifolds), or structural components. In both cases it is not uncommon to drop into airborne or structural borne noise issues (McGary, 1987; Shen et al., 2013; Shin et al., 2020) which directly involve the component's natural frequencies.

This work aims to define differences between the isotropic and anisotropic modeling of PA66GF35 in terms of natural frequencies and vibration modes approaching a historically relevant problem such that of the cantilever square plate. At first instance, a square plate made of PA66GF35, with a thickness of 3 mm and produced by injection moulding process, has been considered. Two numerical models have been developed: in the first model the material was considered as isotropic while, in the second model, it was considered as anisotropic. For the latter model, the injection moulding process was simulated through Autodesk™ Moldflow™ software which, thanks to the implementation of the Folgar and Tucker (1984) theory, allows to obtain the orientation of the fibres within the plate simulating the fluid dynamics of the process. The two models were calibrated by comparing them with an experimental modal analysis performed on the rigidly constrained plate. Differences between the two models (isotropic and anisotropic) were highlighted, showing that while the modal forms are almost unchanged, the differences in the natural frequencies are substantial with a deviation of the order of 10 Hz. The anisotropic behaviour of the plate was also highlighted by performing static tensile tests on samples obtained from the plate and compared with the specimens obtained according to ISO527 standard.

2. Theoretical approach

In this section, a fibre orientation model, developed by Folgar and Tucker, is presented to consider the effect of fibre distribution during the injection mould process. Once the fibre distribution is known, mechanical properties of the composite material can be derived, that is, its local stiffness tensor and thermal expansion coefficient. Finally, the orthotropic cantilever plate vibration problem is presented from an analytical point of view.

2.1 Fibre orientation model

Fibres can be assumed as rigid cylinders with two dimensions (diameter and length) and equally dispersed throughout the volume (uniform concentration of the fibres) (Cintra and Tucker, 1995; Neves et al., 2001). Under these hypotheses the orientation of the single fibre is described through the angles φ and θ, as shown in Figure 1 (Neves et al., 2001).

Since the orientation of the single fibre in a semi-diluted fluid cannot be deterministically described by the field of motion, the more general description of its orientation inside a volume can be described by the probability density function $\psi(\varphi,\theta)$, that is the orientation distribution function. The probability of having a fibre in the domain

$$[\varphi;\varphi+\delta\varphi]\times[\theta;\theta+\delta\theta] \tag{1}$$

is equal to

$$P([\varphi;\varphi+\delta\varphi],[\theta;\theta+\delta\theta]) = \psi(\varphi,\theta)\sin(\theta)d\theta d\varphi \tag{2}$$

The general equation governing time dependency of the orientation distribution function, in the presence of isotropic diffusion ($D\psi$) was derived from Burgers (1938) and it is given by

$$\frac{D\psi}{Dt} = -\nabla(\psi\omega) + D_r\nabla^2\psi \tag{3}$$

where the term ω(φ, θ) represents the angular velocity described by the Jeffery equation (Jeffery, 1922).

If the flow conditions are known throughout the moulding process, the equation can be solved, and the trend

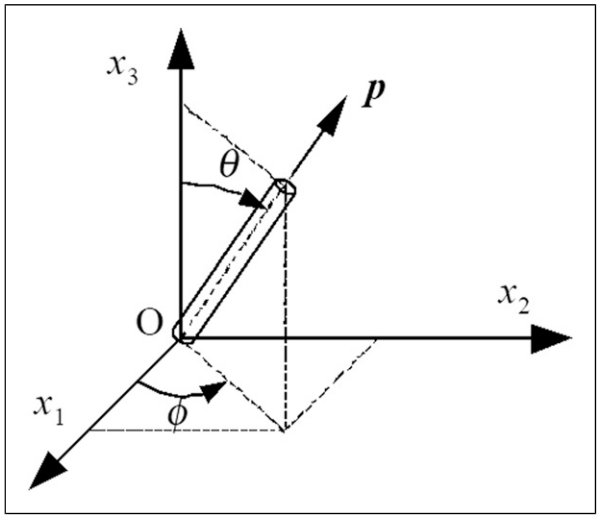

Figure 1. Fibre orientation with respect to the angles φ and θ (Neves et al., 2001).

of the orientation distribution function can then be determined. The function described does not depend only on the components (φ,θ) but also on the spatial position and time in the case of non-stationary flow. It is therefore evident that approach to the solution requires a high computational effort. For the reasons described and in order to obtain a more efficient method to achieve the fibre orientation state, Advani and Tucker (1987) introduced the orientation tensor previously described by Hand (1962). The definitions of the tensor of the second and fourth order are, respectively (Gupta and Wang, 1993)

$$(a_2)_{ij} = \int_{\phi=0}^{2\pi}\int_{\theta=0}^{\pi} p_i p_j \psi(\phi,\theta)\sin\theta d\theta d\phi \tag{4}$$

$$(a_4)_{ijkl} = \int_{\phi=0}^{2\pi}\int_{\theta=0}^{\pi} p_i p_j p_k p_l \psi(\phi,\theta)\sin\theta d\phi \tag{5}$$

where the integrand of equation (4) represents the double product of the vector p, which describes the orientation of the fibre, weighed by the function $\psi(\phi,\theta)$, which represents the probability distribution of finding the fibre in the direction (ϕ,θ). The goal is to determine the terms of the fibre orientation tensor at various points. The theory of Folgar and Tucker (1984) in this sense has the particularity to take into account, in addition to the fluid-dynamic influence (i.e. the flow of the fluid inside the mould), also the interaction that is created between the fibres themselves (situation which occurs in very concentrated fibre-matrix mixtures). Equation (6) expresses the theory described above (Neves et al., 2001)

$$\frac{Da_{ij}}{Dt} = \omega_{ij}a_{kj} - \omega_{kj}a_{ik} + \lambda\left(D_{ik}a_{kj} + D_{kj}a_{ik} - 2D_{kj}a_{ikjl}\right) + 2C_I\dot{\Upsilon}\left(\delta_{ij} - \alpha a_{ij}\right) \tag{6}$$

where λ is the aspect ratio of the fibres, ω_{ij} local vorticity, D_{kj} deformation tensor, δ_{ij} Kronecker delta, α a constant (equal to 3 for three-dimensional flows and 2 for planar flows). The model is valid if the following condition are verified:

- The fibres are rigid cylinders, uniform in length and diameter.
- The fibres are sufficiently large to cause the Brownian motion to be negligible.
- The matrix fluid is so viscous that both particle inertia and particle buoyancy are negligible.
- The centres of mass of the particles are randomly distributed.
- There are no external forces or torques acting on the suspension.

The coefficient C_I is called coefficient of fibre interaction, which is generally determined analytically by the empirical relationship (Neves et al., 2001)

$$C_I = 0.0184^{-0.718\,V_f}\frac{L}{d} \tag{7}$$

where V_f represents the volume fraction of fibres in the matrix, L represents the fibre length and d the fibre diameter. Equation (7) is valid in the concentrated regime, that is, $V_f\frac{L}{d} > 1$.

By resolving the flow field of the fluid within the cast, it is possible to determine the orientation of the fibre at any point in the considered space. Moreover, in the relation, appear both elements of the fourth-order tensor and of the second-order tensor elements which, however, refer to the orientation of the same fibre. For this reason, it is necessary the use of a closure models of the equation that allow to express the terms of the second order according to terms of the fourth. There are different closure models that are used in the calculation of the orientation of the fibres. The choice is a function of the type of flow that is established inside the mould (Parsheh et al., 2006). For example, considering a flow of a poorly deformed polymer with randomly distributed fibres, the Linear Closure model can be used. If, on the other hand, there is a high deformation of the flow and the fibres are aligned in one direction, the Quadratic Closure model can be adopted.

The closure model used for polyamide matrix composite materials is the Orthotropic Closure model (Cintra and Tucker, 1995).

The approximate fourth-order tensor must necessarily be orthotropic, so the main axes of the fourth and second-order tensor must be the same (Cintra and Tucker, 1995). The advantage of this approach lies in the fact that the orthogonal orientation of the tensor makes it diagonal, so many of its components are equal to zero. The fourth-order orthotropic symmetric tensor has nine independent scalar components. Considering the properties of symmetry and normalization, the model proposed by Cintra and Tucker is

$$\begin{aligned} a_{1111} &= f_{11}(a_{11},a_{33}) \qquad a_{2222} = f_{22}(a_{11},a_{33}) \\ a_{3333} &= f_{33}(a_{11},a_{33}) \end{aligned} \tag{8}$$

This model expresses the main components of the fourth-order tensor according to the main components of the second-order tensor. Functions f_{11}, f_{22} and f_{33} are obtained by linear interpolation between the orientation limits of the tensor itself.

Another way to form an orthotropic closure approximation is to choose specific values for the fourth-order components at fixed points and then interpolate between them for all remaining points. The best linear interpolation investigated by Cintra and Tucker, is obtained by considering two configurations: the first 'random-in-plane' (biaxial fibres orientation) with fibres uniformly distributed in a plane, while the latter with 'random-in-space' (triaxial fibres orientation). By linearly interpolating between these states and the uniaxial fibres orientation state, the 'orthotropic smooth closure' equation is obtained (equation (9)) (Cintra and Tucker, 1995)

$$\begin{pmatrix} a_{1111} \\ a_{2222} \\ a_{3333} \end{pmatrix} = \begin{pmatrix} -0.15 + 1,15\ a_{11} - 0.10\ a_{33} \\ +0.60 - 0,6\ a_{11} - 0.6\ a_{33} \\ -0.15 + 1.15\ a_{11} - 0.9\ a_{33} \end{pmatrix} \quad (9)$$

Equation (9) represent the simplest orthotropic form and it is not tied to any model for the physics of fibres orientation, indeed it can be adopted in a wide variety of situations.

2.2 Material mechanical properties

The orientation of the fibres defines certain mechanical properties of the material. The calculation of the effective properties of the fibre/polymer composite involves mediating the properties of the two phases within a finite volume. If the distribution of the fibres is anisotropic, the average process for the stiffness and the coefficient of thermal expansion results in (Burgers, 1938)

$$(K_{ijkl}) = \oint K_{ijkl}\ \psi(p)dp \quad (10)$$

$$(a_{ij}) = \oint a_{ij}\ \psi(p)dp \quad (11)$$

The terms K_{ijkl} and a_{ij} represent the properties of the unidirectional composite, while K_{ijkl} and a_{ij} represent the properties mediated in space considering, through the probability density orientation term $\psi(p)$, the probability to have fibre or not in a certain direction. This procedure, even if analytically correct, presents the disadvantage of determining the volume entity within which to carry out the integral. Advani and Tucker (1987) proposed an alternative expression for calculating the stiffness of the composite and the coefficient of thermal expansion. In the first phase, the coefficients of thermal expansion of the unidirectional composite material, both in longitudinal and transversal directions, are evaluated based on the theory proposed by Schapery (1966, 1970). At the same time the stiffness of the transverse orthotropic composite is determined by referring to the generalized Hooke law. The stiffness of the material is expressed by a 6x6 matrix [C] that relates the strain and stresses (Ting and Ting, 1996)

$$\begin{Bmatrix} \sigma_1 \\ \sigma_2 \\ \sigma_3 \\ \sigma_4 \\ \sigma_5 \\ \sigma_6 \end{Bmatrix} = \begin{bmatrix} c_{11} & \cdots & c_{16} \\ \vdots & \ddots & \vdots \\ c_{61} & \cdots & c_{66} \end{bmatrix} \begin{Bmatrix} \varepsilon_1 \\ \varepsilon_2 \\ \varepsilon_3 \\ \varepsilon_4 \\ \varepsilon_5 \\ \varepsilon_6 \end{Bmatrix} \quad (12)$$

Therefore, assuming the fibres are longitudinally or radially stressed, different material's reaction in terms of stiffness will be obtain, as a function of load direction application. Thus, based on this consideration, it is possible to pass from the condition of anisotropic material to the concept of transversely isotropic material. From the generalized elasticity theory, the stiffness matrix 6x6 of the material becomes (Ting and Ting, 1996)

$$\begin{Bmatrix} \sigma_1 \\ \sigma_2 \\ \sigma_3 \\ \sigma_4 \\ \sigma_5 \\ \sigma_6 \end{Bmatrix} = \begin{bmatrix} c_{11} & c_{12} & c_{13} & 0 & 0 & 0 \\ c_{21} & c_{22} & c_{23} & 0 & 0 & 0 \\ c_{31} & c_{32} & c_{33} & 0 & 0 & 0 \\ 0 & 0 & 0 & c_{44} & 0 & 0 \\ 0 & 0 & 0 & 0 & c_{55} & 0 \\ 0 & 0 & 0 & 0 & 0 & c_{66} \end{bmatrix} \begin{Bmatrix} \varepsilon_1 \\ \varepsilon_2 \\ \varepsilon_3 \\ \varepsilon_4 \\ \varepsilon_5 \\ \varepsilon_6 \end{Bmatrix} \quad (13)$$

where the following relations are valid

$$c_{44} = \frac{1}{2}(c_{22} - c_{23}) \quad (14)$$

$$c_{55} = c_{66} \quad (15)$$

To describe the behaviour of the transversely isotropic material, five elastic constants are necessary that can be determined through the relationships of micromechanics. On the basis of what has been said, it is possible to write the Advani–Tucker relation, which allows to calculate the stiffness of the material using the orientation tensor previously obtained (Gupta and Wang, 1993)

$$\begin{aligned} \langle c_{ijkl} \rangle = {} & B_1 a_{ijkl} + B_2 \left(a_{ij}\delta_{kl} + a_{kl}\delta_{ij} \right) \\ & + B_3 \left(a_{ik}\delta_{ij} + a_{il}\delta_{ik} + a_{jl}\delta_{ik} + a_{jk}\delta_{il} \right) \\ & + B_4 \delta_{jl}\delta_{kl} + B_5 \left(\delta_{ij}\delta_{jl} + \delta_{il}\delta_{jk} \right) \end{aligned} \quad (16)$$

The five quantities B_i are invariant properties of the unidirectional stress tensor. They can be obtained from the unidirectional properties of the transversely isotropic material.

2.3 Orthotropic cantilever plate vibration

From an analytical standpoint, the problem of the free vibration for a cantilever isotropic plate has been considered for many years to be one of the most difficult to solve, because of the free edges. The Rayleigh–Ritz approach was used to obtain accurate results (Chakraverty, 2008). The same method was applied to the problem of the orthotropic rectangular cantilever plate with considerable success, although it was admitted that the conditions of free edges could never be met exactly. The accurate solution of cantilever plate with rectangular orthotropy was proposed by Gorman (1995) with the superposition method (Hand, 1962).

In the case of rectangular orthotropy the governing differential equation is

Table 1. PA66GF35 mechanical and thermal properties as declared by the manufacturer (Crupi et al., 2015).

Tensile strength σ_u (MPa)	Young's modulus E (GPa)	Fibre length L (μm)	Fibre diameter d (μm)	Poisson ratio ν [-]	Density ρ (kg/m^3)	Specific heat c_p (J/kg.K)
150–210	8.7–11.4	280	10	0.39	1410	1670

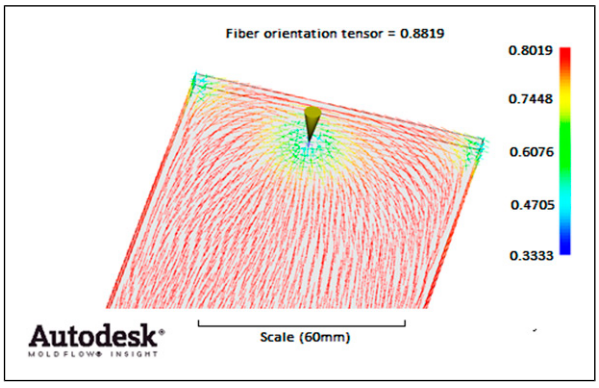

Figure 2. Injection process simulated using Autodesk™ Moldflow™ software. The yellow cone represents the injection point, while the colour bar the fibre orientation tensor.

$$\frac{\partial^4 W(\xi,\eta)}{\partial\eta^4} + 2\frac{H}{D_y}\varphi^2\frac{\partial^4 W(\xi,\eta)}{\partial\xi^2\partial\eta^2} + \frac{D_x}{D_y}\varphi^4\left\{\frac{\partial^4 W(\xi,\eta)}{\partial\xi^4} - \lambda^4 W(\xi,\eta)\right\} = 0 \tag{17}$$

where all the symbols are listed in nomenclature.

From equation (17), it is possible to compute the eigenvalues λ^2, which represents the vibration mode, in function of the aspect ratio φ of the plate. In this work, the attention is focused on the first four vibration mode of the cantilever plate.

3. Material and methods

3.1 Numerical model

The composite material under study was a PA66GF35, with an aliphatic polyamide 66 matrix and glass fibres dispersed in the matrix with a weight percentage of 35%. Table 1 reports the mechanical properties as declared by the manufacturer. These values were implemented in Finite Element Method (FEM) analysis for the isotropic model. By injection moulding a square plate was realized, whose dimensions are 200 mm × 200 mm × 3 mm. The analysis of the dynamic behaviour of the plate and its mechanical properties were numerically investigated and experimentally validated.

Numerical investigations were carried out considering the plate with both isotropic and anisotropic behaviour. Based on the material properties declared by the manufacturer, the authors have been implemented in the FEM model, for the isotropic case, the mean value of the tensile strength and the Young's modulus: $\sigma_u = 180\ MPa$ and $E = 10.5\ GPa$. For the anisotropic case, Folgar and Tucker model was adopted to obtain the fibre orientation within the plate, firstly determining the fluid-dynamic behaviour of the polymer injected into the mould, from which the fibre orientation tensor was obtained, and subsequently deriving the stiffness of each individual element in the discretized domain. The injection process was simulated using Autodesk™ Moldflow™ software (Figure 2) which implements Folgar and Tucker (1984) theory and resolves, in the considered space domain, injection fluid dynamics.

From MoldFlow™ software, a mesh file with the mechanical properties, that is, the stiffness tensor of each finite element, was retrieved and then imported into Ansys™ for the calculation of the vibrating modes in the cantilever plate configuration. Finite element simulations were carried out with Ansys® software adopting SHELL181 elements. It is a four-node element with six degrees of freedom at each node: translation and rotation about x, y and z axis. After carrying out a convergence analysis (Patil and Jeyakarthikeyan, 2018; Valeš and Kala, 2018) on the mesh size, the element's dimension adopted for the simulation was 2 mm.

Knowing the mass $[m]$ and stiffness $[k]$ matrices of the component, through the following equation

$$det\left[[m]s^2 + [k]\right] = 0 \tag{18}$$

it is possible to obtain the natural frequencies $[\omega_0^2]$ and the modal forms $[\varphi]$ of the system that allows to characterize the plate dynamically. The difference between the two models of the material under consideration, isotropic and anisotropic, is based on this aspect. Indeed, while for the isotropic material, it is possible to carry out a modal analysis by defining only the Young's modulus and the Poisson's ratio. To describe the anisotropic material, it is necessary to resolve the fluid-dynamic of the injection process and derive the stiffness tensor distribution in every point of the plate.

Clearly, the difference between the two models is reflected in a different matrix of modal participation coefficients.

3.2 Experimental setup

An experimental modal analysis was performed to compare the real behaviour of the plate with the results obtained by Finite Element (FE) analysis. The plate was fixed along the side where the injection takes place (Figure 3).

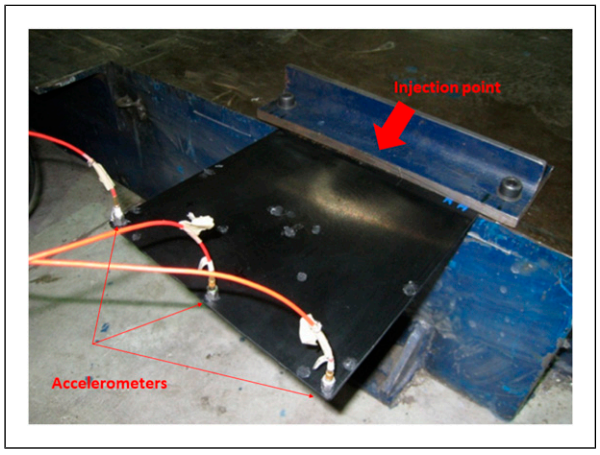

Figure 3. Testing system for the anisotropic cantilever plate.

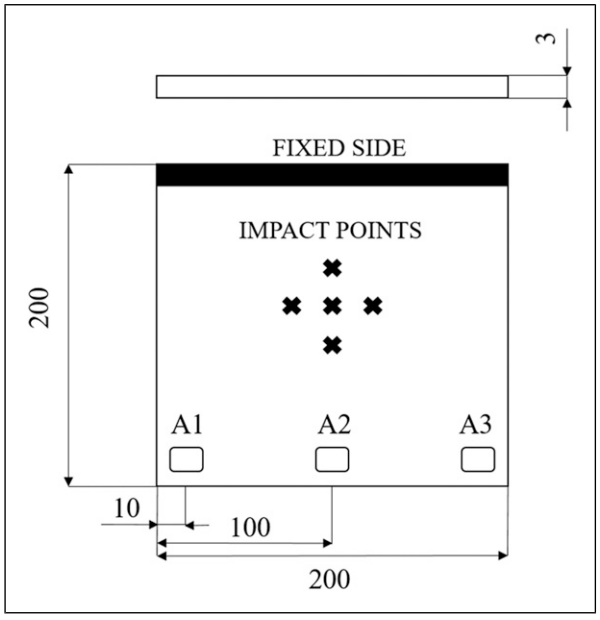

Figure 4. Schematic view of the plate with accelerometer position and impact points.

The experimental apparatus is a Hammer Impact Test System of Prosig® company (Fareham, UK). It consists of an instrumented hammer, triaxial piezoelectric accelerometer and acquisition unit (model P8012 with DATS software to visualize and processing data).

For the experimental modal analysis, different points were considered for the application of the impulse in order to obtain an adequate frequency response (Figure 4).

The choice of the impact points is related to the following equation

$$H_{ij} = \sum_{i=1}^{n} \phi_{ir}\phi_{jr}H_r \tag{19}$$

The function represents the response in the frequency domain of the j-th point to the application of the force in the i-th point. The H_r function represents the frequency response of the systems to a degree of freedom that can be obtained from the modal analysis, in which each system has a resonance frequency ω_r. Hence, in order to observe a particular frequency response, it is necessary to excite and measure the response of the structure where the product $\varphi_{ir}\varphi_{jr}$ is maximum. These coefficients respectively represent the coefficient of modal participation of the measurement point and impact point of the impulse.

3.3 Tensile test

To confirm the anisotropic behaviour of the composite material PA66GF35, static tensile tests were performed both on a set of specimens realized directly by injection moulding, according to ISO527-2:1993 standard (type 1A specimen) (Crupi et al., 2015) (Figure 5(a)), and on samples obtained by sectioning the plate along and orthogonal to the injection direction (Figure 5(b)).

The static tensile tests were performed under displacement control, with a crosshead speed of 3 mm/min, adopting a servo-hydraulic test machine ITALSIGMA 25 kN (Figure 5(c)).

The injection moulding conditions are based on ISO 294-1:1996 and ISO 1873-2:2007 standard, and the main constructional details of ISO moulds used to produce 1A type specimen are as follows:

- The sprue diameter on the nozzle side shall be at least 4 mm.
- The width and height (or the diameter) of the runner system shall be at least 5 mm.
- The height of the gate shall be at least two-thirds the height of the cavity, and the width of the gate shall be the point where the gate enters the cavity.
- The gate shall be as short as possible, in any case not exceeding 3 mm.
- The draft angle of the runners shall be at least 10°, but not more than 30°. The cavity shall have a draft angle not greater than 1 degree, except in the area of tensile specimen shoulders where the draft angle shall not be greater than 2°.
- The heating/cooling system for the mould plates shall be designed so that, under operating conditions, the difference in temperature between any point on the surface of a cavity and either plate is less than 5°C.

4. Results and discussions

From the numerical analysis, the modal forms of the plate have been investigated both for isotropic (Figure 6(a)–(d)) and anisotropic (Figure 7(a)–(d)) material models. Tables 2 and 3 shows the natural frequencies computed values for isotropic and anisotropic model, respectively. As can be seen from Figures 7 and 8, the modal forms (Mode 1–2) are

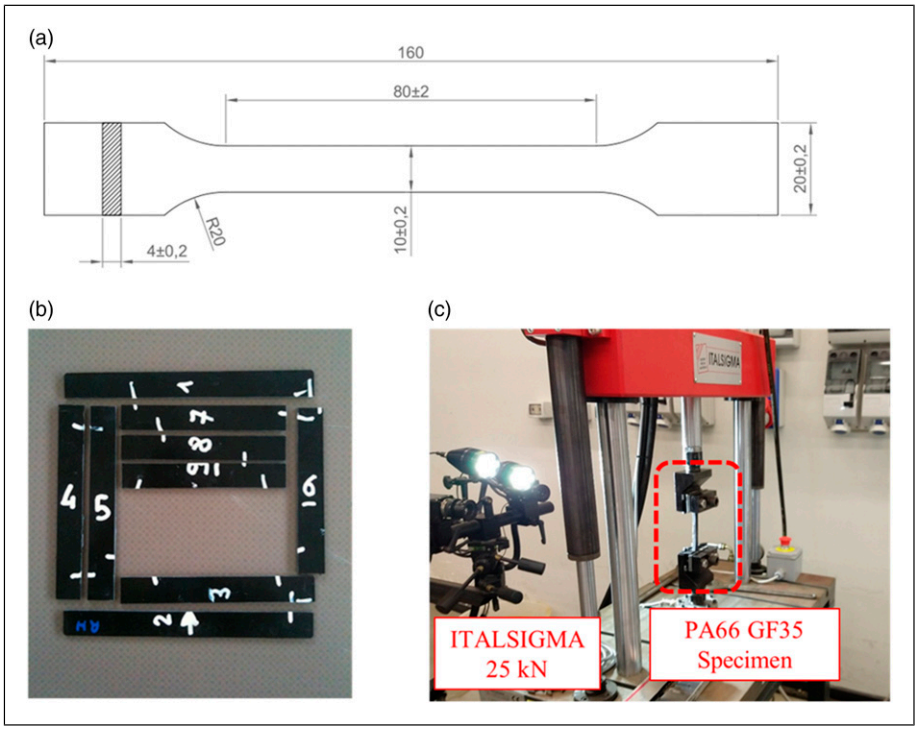

Figure 5. (a) PA66GF35 specimen realized according to ISO527 standard; (b) Plate samples extracted in parallel and orthogonal direction with respect to the injection point (white arrow); (c) servo-hydraulic test machine ITALSIGMA.

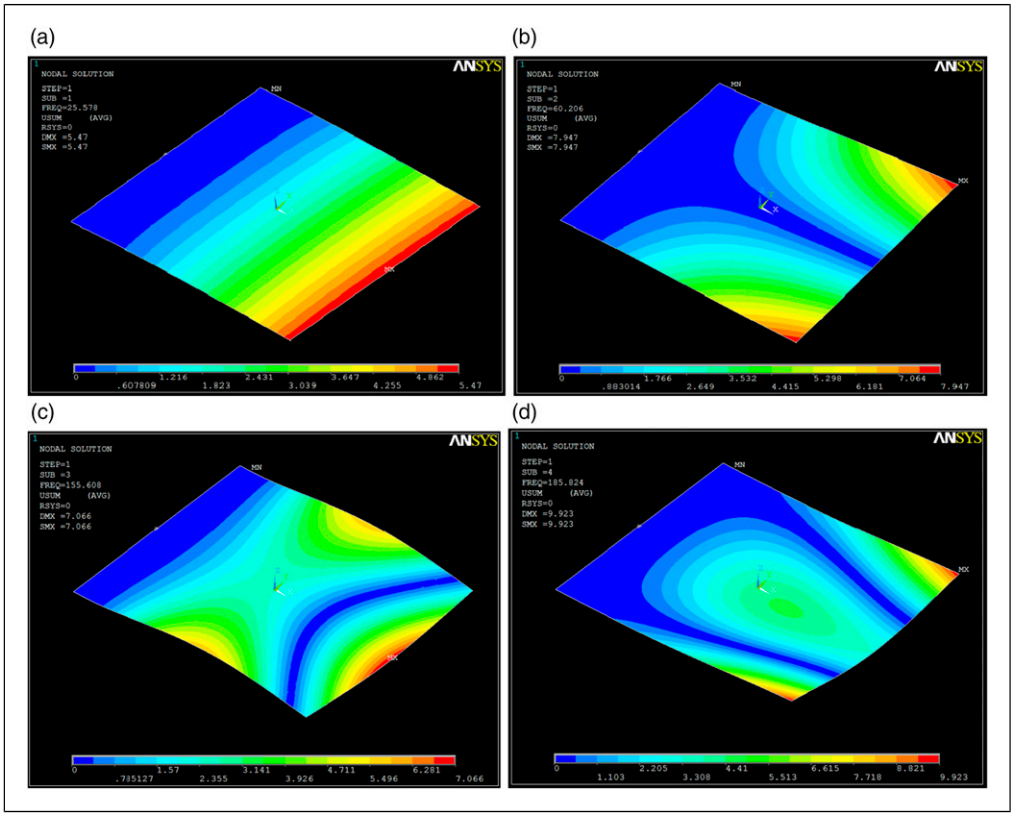

Figure 6. Modal forms of the plate evaluated trough FE analysis for the isotropic model. Colour bar values represents the deflection in mm. (a) First mode (b) Second mode (c) Third mode (d) Fourth mode.

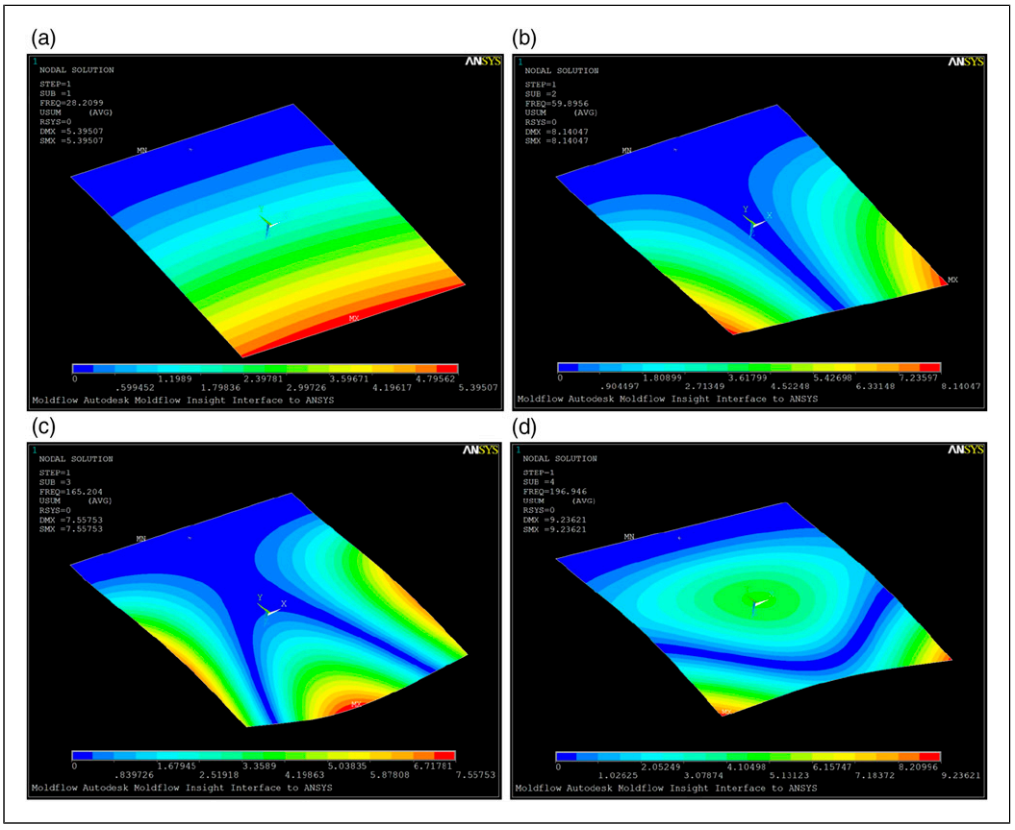

Figure 7. Modal forms of the plate evaluated trough FE analysis for the anisotropic model. Colour bar values represents the deflection in mm. (a) First mode (b) Second mode (c) Third mode (d) Fourth mode.

Table 2. Natural frequencies computed from FEM analysis for the isotropic model.

No. mode	Value (Hz)
1	25.58
2	60.21
3	155.61
4	185.83

Table 3. Natural frequencies computed from FEM analysis for the anisotropic model.

No. mode	Value (Hz)
1	28.21
2	59.9
3	165.2
4	196.95

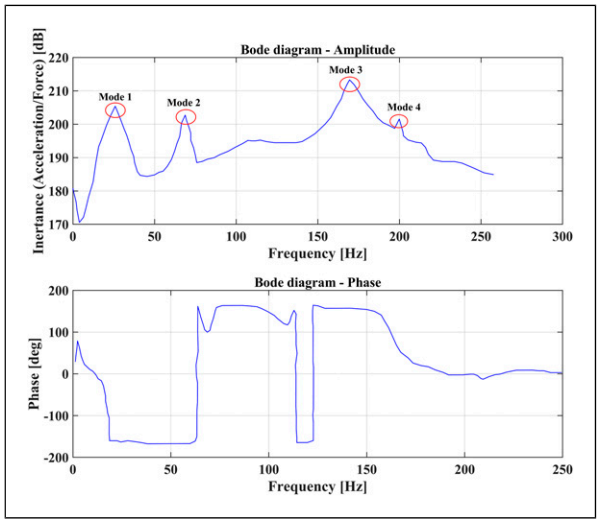

Figure 8. Bode diagram (amplitude and phase) extracted from experimental modal test.

almost unchanged in the isotropic case and in the anisotropic case, since the variation in the orientation of the fibres significantly affect only the modes of vibrations at higher frequencies of the system. This happens because, at higher frequencies, the local properties of the material become predominant. Hence, the isotropic model is expected to exhibit a larger deviation from the experimental results. On the other hand, the anisotropic model, which intrinsically

Table 4. Different vibration modes of the plate obtained through FE and experimental analysis.

No. mode	Experimental test (Hz)	Anisotropic FE model (Folgar and Tucker) (Hz)	Isotropic FE model (Hz)
1	25	28	26
2	63	60	60
3	168	165	155
4	193	197	186

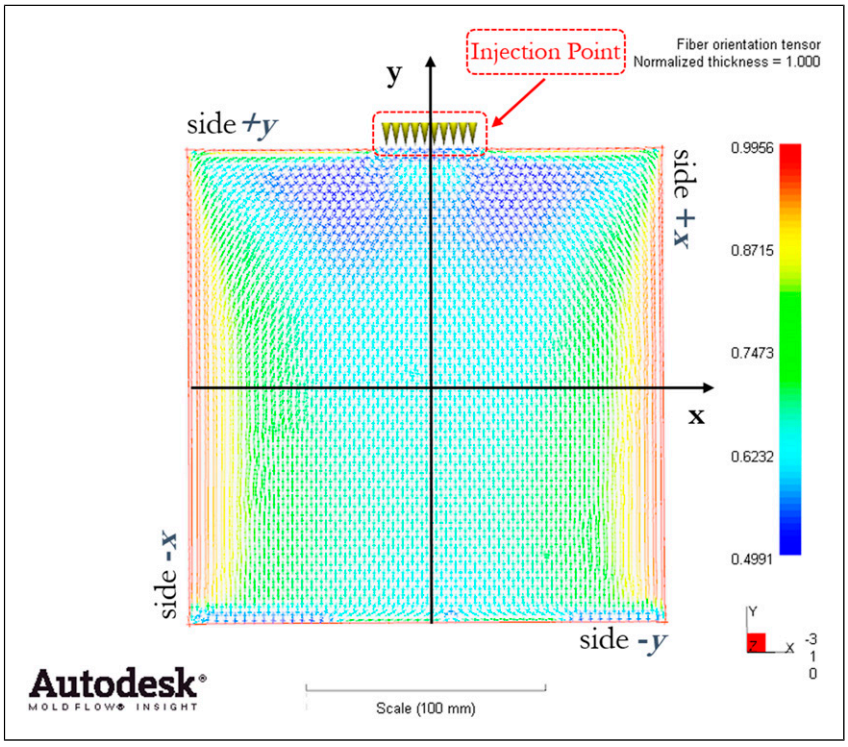

Figure 9. Arrangement of the glass fibres in the polyamide matrix and different constrain condition.

Table 5. Comparison between the vibration modes obtained from numerical simulation for different interlocking sides.

No. mode	Fixed side +y	Fixed side −y	Fixed side −x	Fixed side +x
1	28	32	23	23
2	60	63	59	59
3	165	165	145	145
4	197	197	206	206

consider the stochastic orientation of the fibre, shows a good agreement with the experimental results, also at high frequencies.

The experimental modal analysis consists of five tests aimed to establish the vibration modes of the plate. To compare the experimental modal analysis with the numerical one, the most representative result has been taken into account. Figure 8 shows the bode diagram with the inertance, that is, the ratio between acceleration and force, and phase angle versus frequency. Moreover, considering the high sensitivity of the experimental setup to noise and vibration, the output signal has been filtered with MATLAB™ using a lowpass filter to highlights the vibration modes of the plate.

As can be seen from Figure 7, the four main experimental modes of vibration of the plate are circled in red: 25 Hz, 63 Hz, 168 Hz and 193 Hz, respectively. Table 4 reports the comparison between numerical and experimental vibration modes of the plate. The difference between the vibration modes of the plate obtained through FE analysis

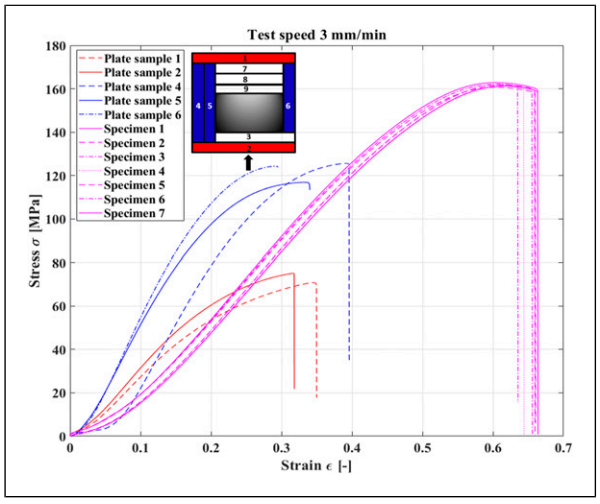

Figure 10. Tensile static test carried out both on samples extracted from the plate and specimen realized according to ISO527 standard.

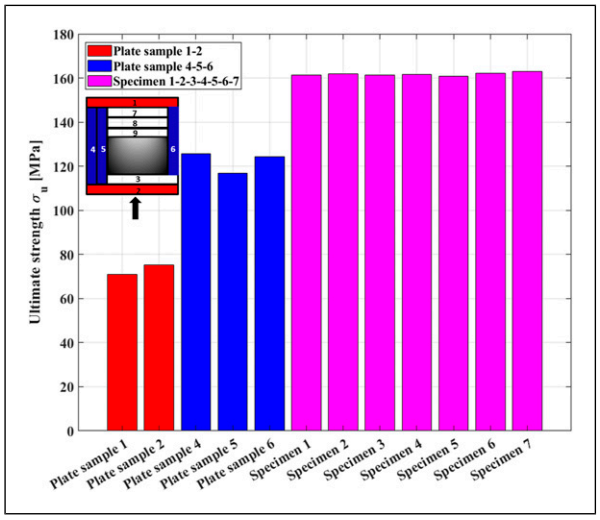

Figure 11. Evidence of the material's anisotropy on ultimate strength.

considering an anisotropic material using Folgar and Tucker model, and experimental analysis settles around 3 Hz. The model, therefore, can be considered calibrated.

Interesting results concern the variation of frequencies. Indeed, as shown in Table 4, the differences are small at low frequencies but become substantial at higher frequencies. The anisotropic model is in good agreement with the experimental test while the isotropic model presents a deviation of about −8%. Whereas this material is mainly employed for the production of intake manifold, where the engine rotation regimes are around 7000–8000 rpm (Harrison and Dunkley, 2004), is evident why the attention is focused on higher frequencies. For this reason, the anisotropic model represents the best choice to approximate the real behaviour of the plate.

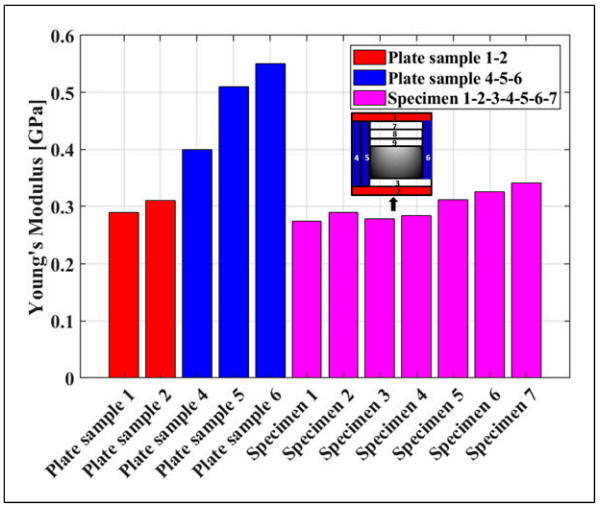

Figure 12. Evidence of the material's anisotropy on Young's modulus.

The anisotropy of the material is derived from the fluid dynamics of the injection moulding process and, therefore, from the arrangement of the glass fibres within the polyamide matrix (Figure 9). Considering the agreement between the anisotropic FE model and the experimental test, the numerical model has been considered calibrated. Hence, it is also possible to investigate the effect the interlocking side change have on the vibration modes. If the interlocking side is changed in FE simulations, it is possible to observe a certain dispersion (Table 5) on the vibration modes.

In fact, apart the same results for the symmetric sides (+x, −x and +y, −y), the vibration modes are very different between one case and another (for example, +x and +y), up to 20 Hz in the case of mode 3. It is therefore evident the strong anisotropy of short-fibre composite materials and how, by simply changing the constraint conditions, the results differ greatly from each other.

To further confirm the anisotropy of the plate, static tensile tests were carried out both on samples extracted from the plate and specimen realized directly by injection moulding, according to ISO527-2:1993 standard.

As can be seen in Figure 10, the strong anisotropy of the material is reflected on different σ-ε curves and, consequently, on a different Ultimate strength σ_u (Figure 11). The Ultimate strength has been evaluated as the maximum stress value obtained from the experimental test. The stress σ has been evaluated as the ratio between the applied force on the specimen/plate sample and the nominal cross-sectional area. The strain ε have been evaluated has the ratio between the elongation which specimen/plate sample undergoes and the initial gauge length (L_0 = 50 mm) of an extensometer. The main influence on the anisotropy is, of course, given by the fibre directions which depends on the injection point. This is confirmed by the comparison between the plate samples extracted in parallel and orthogonal

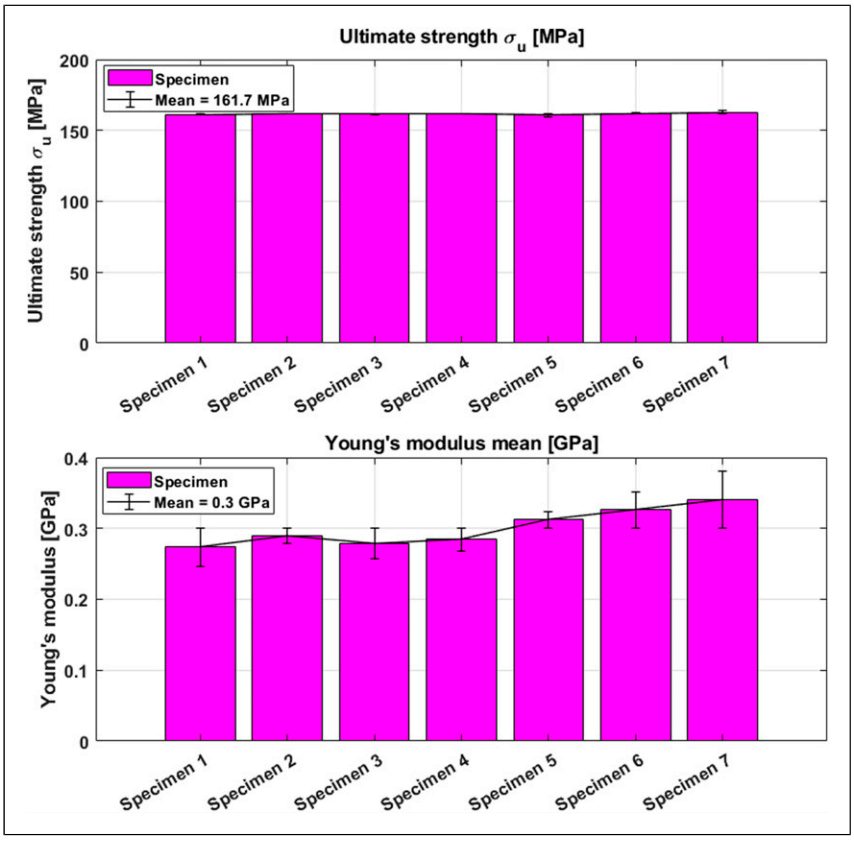

Figure 13. Error between experimental mean value and experimental individual values.

direction with respect to the injection point. The first ones in fact have greater Ultimate strength σ_u (plate samples 4-5-6).

The mechanical strength of the material strongly depends on the dimension and type of mould of the realized specimen, and hence on the real application (component) of the material. In fact, the specimens realized according to standard exhibits greater Ultimate strength σ_u compared to the plate samples (Figure 11). The stress-strain curves exhibit a first small linear trend part, due to the arrangement of the testing machine clamping system, and a second more marked linear trend. The young's modulus has been evaluated considering the linear regression of the stress versus strain points within the second linear trend part of the curve, prior to the plateau region.

The investigation about Young's modulus (Figure 12) shows that the plate samples extracted along the injection direction presents a greater Young's modulus (and hence a greater stiffness) with respect the plate samples extracted along the orthogonal direction, and also compared with the specimens.

All these considerations confirm that the composite material cannot be considered isotropic, as it is normally considered in industrial applications. Moreover, if the field of application makes the component's dimension and the mould type far from the regulation, it is not possible to relate the mechanical strength from static tensile specimens, obtained according to the standard, to the one of the real components.

Finally, mean and standard deviation of Ultimate strength and Young's modulus of the ISO527 specimens has been evaluated. Figure 13 shows the error between experimental mean value and experimental individual values (Ultimate strength and Young's modulus). The computed values of standard deviation regarding Ultimate strength and Young's modulus are respectively $\sigma_{\sigma_u} = 0.0098$ and $\sigma_E = 0.6748$.

5. Conclusion

The anisotropic behaviour of the PA66GF35 composite material has been investigated by numerical and experimental analyses. The injection moulding process of a plate was simulated through Autodesk^{TM} Moldflow^{TM} software, implementing Folgar and Tucker's theory. This allows to obtain the fibres orientation due to fluid-dynamics phenomena which occurs inside the mould. Two numerical models of the constrained plate have been implemented to obtain the frequency response: the first model implements an isotropic material behaviour; while the latter an anisotropic behaviour. The numerical models were calibrated by

comparing them with an experimental modal analysis performed on a constrained cantilever plate. The two models (isotropic and anisotropic) were compared, showing that while the modal forms are almost unchanged, the differences in the natural frequencies are substantial, with a deviation of about 8 Hz.

By changing the constrained side of the plate, numerical natural frequency results show a high dispersion, function of the different arrangement of the fibres, up to a difference of 20 Hz for mode 3.

Finally, to confirm the anisotropic behaviour of the PA66GF35 composite plate, static tensile tests were carried out both on samples extracted from the plate and on specimens realized according to ISO527 standard, highlighting the low values of the ultimate strength for the samples that have an orthogonal arrangement of the fibres. Since composite materials are also adopted to make components in the automotive and transport fields significantly affected by airborne and solidborne noise problems, it is easy to understand what role the natural frequencies and the modes of vibration play in these cases. In fact, with the same geometry, it is unequivocally that the material influences the system's own frequencies. Therefore, as shown in this study, incorrect modeling of the material, usually assumed isotropic, leads to an incorrect estimate of noise problems. Moreover, from the comparison between the plate samples extracted along the injection direction and the standard specimen, it is evident how the mould geometry and process conditions influence the mechanical strength of the component. Indeed, despite the material is the same for both cases (plate sample and standard specimens) differences in ultimate strength and tensile modulus have been observed. This means that, when this material is employed to produce real component, it is necessary to take into account during the design phase a certain deviation from the mechanical features evaluated from standard specification. For this reason, future works will focus on modal analysis of complex components, such as intake manifold, to correlate the real behaviour of the component with respect to the base material.

Author contributions

Lorenzo Scappaticci: Writing-Original Draft; Conceptualization; Supervision; Validation. Fabio Alberti: Formal analysis; Investigation; Methodology; Data curation; Writing-Original Draft; Writing - Review & Editing. Giacomo Risitano: Conceptualization; Supervision; Validation. Dario Santonocito: Data curation; Writing - Review & Editing. Danilo D'Andrea: Formal analysis; Investigation; Methodology; Data curation; Writing-Original Draft; Writing - Review & Editing.

Declaration of Conflicting Interests

The author(s) declared no potential conflicts of interest with respect to the research, authorship, and/or publication of this article.

Funding

The author(s) received no financial support for the research, authorship, and/or publication of this article.

ORCID iD

Danilo D'Andrea https://orcid.org/0000-0002-9809-8434

References

Advani SG and Tucker CL, III (1987) The use of tensors to describe and predict fiber orientation in short fiber composites. *Journal of Rheology* 31(8): 751–784.

Anandakumar P, Timmaraju MV and Velmurugan R (2021) Development of efficient short/continuous fiber thermoplastic composite automobile suspension upper control arm. *Materials Today: Proceedings* 39: 1187–1191. DOI: 10.1016/j.matpr.2020.03.543.

Bernasconi A, Davoli P, Basile A, et al. (2007) Effect of fibre orientation on the fatigue behaviour of a short glass fibre reinforced polyamide-6. *International Journal of Fatigue* 29(2): 199–208. DOI: 10.1016/j.ijfatigue.2006.04.001.

Bernasconi A, Cosmi F and Dreossi D (2008) Local anisotropy analysis of injection moulded fibre reinforced polymer composites. *Composites Science and Technology* 68(12): 2574–2581. DOI: 10.1016/j.compscitech.2008.05.022.

Bigg DM (1985) Effect of compounding on the properties of short fiber reinforced injection moldable thermoplastic composites. *Polymer Composites* 6(1): 20–28. DOI: 10.1002/pc.750060105.

Burgers J (1938) *Second Report on Viscosity and Plasticity*. New York, NY: Nordemann, p. 113.

Caltagirone PE, Ginder RS, Ozcan S, et al. (2021) Substitution of virgin carbon fiber with low-cost recycled fiber in automotive grade injection molding polyamide 66 for equivalent composite mechanical performance with improved sustainability. *Composites Part B: Engineering* 221: 109007. DOI: 10.1016/j.compositesb.2021.109007.

Chakraverty S (2008) Background of vibration. In: *Vibration of Plates*. Boca Raton, FL: CRC Press, 1–32. DOI: 10.1115/1.801993.ch7.

Cintra JS, Jr and Tucker CL, III (1995) Orthotropic closure approximations for flow-induced fiber orientation. *Journal of Rheology* 39(6): 1095–1122.

Crupi V, Guglielmino E, Risitano G, et al. (2015) Experimental analyses of SFRP material under static and fatigue loading by means of thermographic and DIC techniques. *Composites Part B: Engineering* 77: 268–277. DOI: 10.1016/j.compositesb.2015.03.052.

Cucinotta F, Guglielmino E, Risitano G, et al. (2016) Assessment of damage evolution in sandwich composite material subjected to repeated impacts by means optical measurements. *Procedia Structural Integrity* 2: 3660–3667. DOI: 10.1016/j.prostr.2016.06.455.

De Monte M, Moosbrugger E and Quaresimin M (2010) Influence of temperature and thickness on the off-axis behaviour of short glass fibre reinforced polyamide 6.6 - Cyclic loading. *Composites Part A: Applied Science and Manufacturing* 41(10): 1368–1379. DOI: 10.1016/j.compositesa.2010.02.004.

Folgar F and Tucker CL (1984) Orientation behavior of fibers in concentrated suspensions. *Journal of Reinforced Plastics and Composites* 3(2): 98–119. DOI: 10.1177/073168448400300201.

Fu H, Xu H, Liu Y, et al. (2020) Overview of injection molding technology for processing polymers and their composites. *ES Materials & Manufacturing* 8: 3–23. DOI: 10.30919/esmm5f713.

Gibson RF (2000) Modal vibration response measurements for characterization of composite materials and structures. *Composites Science and Technology* 60(15): 2769–2780. DOI: 10.1016/S0266-3538(00)00092-0.

Gorman DJ (1995) Accurate free vibration analysis of the orthotropic cantilever plate. *Journal of Sound and Vibration* 181(4): 605–618. DOI: 10.1006/jsvi.1995.0161.

Gupta M and Wang KK (1993) Fiber orientation and mechanical properties of short-fiber-reinforced injection-molded composites: simulated and experimental results. *Polymer Composites* 14(5): 367–382. DOI: 10.1002/pc.750140503.

Hand GL (1962) A theory of anisotropic fluids. *Journal of Fluid Mechanics* 13(1): 33–46.

Hao X, Zhou H, Mu B, et al. (2020) Effects of fiber geometry and orientation distribution on the anisotropy of mechanical properties, creep behavior, and thermal expansion of natural fiber/HDPE composites. *Composites Part B: Engineering* 185: 107778. DOI: 10.1016/j.compositesb.2020.107778.

Harrison MF and Dunkley A (2004) The acoustics of racing engine intake systems. *Journal of Sound and Vibration* 271: 959–984. DOI: 10.1016/S0022-460X(03)00773-9.

Hmeidat NS, Pack RC, Talley SJ, et al. (2020) Mechanical anisotropy in polymer composites produced by material extrusion additive manufacturing. *Additive Manufacturing* 34: 101385. DOI: 10.1016/j.addma.2020.101385.

Inoue Y, Ikawa T and Okabe T (2019) Validation of micromechanics models including imperfect interfaces for short fiber thermoplastic composites. *Advanced Composite Materials* 28(6): 625–638. DOI: 10.1080/09243046.2019.1630049.

Jeffery GB (1922) The motion of ellipsoidal particles immersed in a viscous fluid. *Proceedings of the Royal Society A* 102(715): 161–179.

Kuo PY, Wang SY, Chen JH, et al. (2009) Effects of material compositions on the mechanical properties of wood-plastic composites manufactured by injection molding. *Materials and Design* 30(9): 3489–3496. DOI: 10.1016/j.matdes.2009.03.012.

Launay A, Marco Y, Maitournam MH, et al. (2010) Cyclic behavior of short glass fiber reinforced polyamide for fatigue life prediction of automotive components. *Procedia Engineering* 2(1): 901–910. DOI: 10.1016/j.proeng.2010.03.097.

Lopes PAM, Gomes HM and Awruch AM (2010) Reliability analysis of laminated composite structures using finite elements and neural networks. *Composite Structures* 92(7): 1603–1613. DOI: 10.1016/j.compstruct.2009.11.023.

Martinez JR and Bishay PL (2021) On the stochastic first-ply failure analysis of laminated composite plates under in-plane tensile loading. *Composites Part C: Open Access* 4: 100102. DOI: 10.1016/j.jcomc.2020.100102.

McGary MC (1987) Interaction of airborne and structure-borne noise radiated by plates. *Journal of Sound and Vibration* 115(3): 387–403. DOI: 10.1016/0022-460X(87)90285-9.

Mortazavian S and Fatemi A (2015) Effects of fiber orientation and anisotropy on tensile strength and elastic modulus of short fiber reinforced polymer composites. *Composites Part B: Engineering* 72: 116–129. DOI: 10.1016/j.compositesb.2014.11.041.

Mouti Z, Westwood K, Kayvantash K, et al. (2010) Low velocity impact behavior of glass filled fiber-reinforced thermoplastic engine components. *Materials* 3(4): 2463–2473. DOI: 10.3390/ma3042463.

Neves NM, Pontes AJ and Pouzada AS (2001) Experimental validation of morphology simulation in glass fibre reinforced polycarbonate discs. *Journal of Reinforced Plastics and Composites* 20(6): 452–465.

Onkar AK, Upadhyay CS and Yadav D (2007) Probabilistic failure of laminated composite plates using the stochastic finite element method. *Composite Structures* 77(1): 79–91. DOI: 10.1016/j.compstruct.2005.06.006.

Parsheh M, Brown ML and Aidun CK (2006) Investigation of closure approximations for fiber orientation distribution in contracting turbulent flow. *Journal of Non-newtonian Fluid Mechanics* 136(1): 38–49.

Patil H and Jeyakarthikeyan P V (2018) Mesh convergence study and estimation of discretization error of hub in clutch disc with integration of ANSYS. *IOP Conference Series: Materials Science and Engineering* 402(1): 012065. DOI: 10.1088/1757-899X/402/1/012065.

Schapery RA (1966) An engineering theory of nonlinear viscoelasticity with applications. *International Journal of Solids and Structures* 2(3): 407–425.

Schapery RA (1970) On a thermodynamic constitutive theory and its application to various nonlinear materials. In Thermoinelasticity (pp. 259-285). Springer, Vienna.

Shen C, Xin FX, Cheng L, et al. (2013) Sound radiation of orthogonally stiffened laminated composite plates under airborne and structure borne excitations. *Composites Science and Technology* 84: 51–57. DOI: 10.1016/j.compscitech.2013.05.006.

Shin P-S, Kim J-H, DeVries K-L, et al. (2020) Manufacturing and qualitative properties of glass fiber/epoxy composite boards with added air bubbles for airborne and solid-borne sound insulation. *Composites Science and Technology* 194: 108166. DOI: 10.1016/j.compscitech.2020.108166.

Tawfik ME, Bishay PL and Sadek EE (2018) Neural network-based second order reliability method (NNBSORM) for laminated composite plates in free vibration. *CMES - Computer Modeling in Engineering and Sciences* 115(1): 105–129. DOI: 10.3970/cmes.2018.115.105.

Ting TC and Ting TC (1996) *Anisotropic Elasticity: Theory and Applications*. Oxford, UK: Oxford University Press.

Treviso A, Van Genechten B, Mundo D, et al. (2015) Damping in composite materials: properties and models. *Composites Part B: Engineering* 78: 144–152. DOI: 10.1016/j.compositesb.2015.03.081.

Vaidya UK and Chawla KK (2008) Processing of fibre reinforced thermoplastic composites. *International Materials Reviews* 53(4): 185–218. DOI: 10.1179/174328008X325223.

Valeš J and Kala Z (2018) Mesh convergence study of solid FE model for buckling analysis. *AIP Conference Proceedings* 1978: 150005. DOI: 10.1063/1.5043796.

Wu S-H, Wang F-Y, Ma CCM, et al. (2001) Mechanical, thermal and morphological properties of glass fiber and carbon fiber reinforced polyamide-6 and polyamide-6/clay nano-composites. *Materials Letters* 49(6): 327–333. DOI: 10.1016/S0167-577X(00)00394-3.

Ye H, Liu XY and Hong H (2008) Fabrication of metal matrix composites by metal injection molding-A review. *Journal of Materials Processing Technology* 200(1–3): 12–24. DOI: 10.1016/j.jmatprotec.2007.10.066.

Appendix

Nomenclature

φ	$= b/a$ aspect ratio of the plate [−]
ϕ	Orientation angle of the fibre in x_1-x_2 plane [deg]
θ	Orientation angle of the fibre in x_2-x_3 plane [deg]
v_x,v_y	Poisson ratios associated with x and y directions [−]
ω	Angular velocity [rad/s]
ξ,η	$= x/a$ and y/b respectively [−]
$\psi(\varphi,\theta)$	Orientation distribution function
λ^2	Eigenvalues for the first four modes [rad m^2/s (kg/m^3Nm^2)$^{1/2}$]
$[\sigma]$	Stress matrix [MPa]
$[\varepsilon]$	Strain matrix [−]
$\dot{\Upsilon}$	Magnitude of the strain rate tensor [s^{-1}]
a,b	Edge length of half plate [m]
$[C]$	Stiffness matrix [N/m]
d	Diameter of the fibre [m]
D_r	Isotropic rotary diffusivity [rad^2/s]
D_t	Torsional rigidity of orthotropic plate [Nm/rad]
D_x,D_y	Flexural rigidities associated with x and y directions of orthotropic plate [Nm^2]
H	$2H = v_yD_x + v_xD_y + 4D_t$
L	Length of the fibre [m]
p	Vector describing fibre orientation
V_f	Volume fraction of the fibre in the matrix [%]
W	Plate lateral displacement divided by a [−]